

Didymoon's surface thermal modeling

Grégoire Henry

Royal observatory of Belgium

Institut Polytechnique des Sciences Avancées

2019

Abstract

Didymoon is an asteroid of the binary system Didymos. It is orbiting around a bigger asteroid called Didymain for convenience. In order to prepare the defense of the Earth in the case of a direct impact of an asteroid, the Hera mission will initiate in the years to follow an impact onto Didymoon. The NASA is in charge of the collision with the asteroid. The ESA will study the outcomes of the impact. The spacecraft Hera will be equipped of sensors such as cameras. Studying the evolution of the temperature on Didymoon will help us to understand what happened to after the collision. This work fits into the scheme of the simulations of thermal camera images from the spacecraft around the asteroid. This paper shows a method using asteroid thermophysical model, 1D numerical solver, NASA/NAIF SPICE and shape models.

Introduction

Binary systems are frequent among the near-Earth asteroid population: the fraction of binaries larger than 300 m was estimated to be $15 \pm 4\%$. The study of binary systems is important for space missions, such as the Asteroid Impact Mission (AIM), that target the primary or secondary asteroidal body. The binary nature of Apollo class asteroid 65803 Didymos was discovered in 1996. Didymos is a close binary system, consisting of a larger primary (780 m diameter $\pm 10\%$) and a smaller (163 m ± 18 m across) secondary. Didymos' heliocentric eccentricity is reported as 0.38, the semi-major axis is 1.64 AU and the inclination to the ecliptic is 3.4 degrees. The orbital period of Didymoon is determined as 11.92 hours. The rotational period of the main body is 2.6 hours and the secondary's rotational period appears to be 11.92 hours as well, i.e. a synchronous rotation.

Didymoon will be impacted by the NASA DART space-craft in October 2022. Its orbital velocity of about 17 cm/s is expected to be shifted by around half a millimetre per second, changing its rotation period around the primary body by about 200 seconds – a fraction of one per cent, but enough to be measured roughly with Earth-based telescopes. Hera will map Didymoon's entire surface down to a size resolution of a few metres, and the tenth of the surface surrounding the DART crater down to better than 10 cm resolution, through a series of daring flybys. It will also map much of the surface of the primary Didymos asteroid, providing crucial scientific

data from two asteroids in a single mission.

This document presents the thermophysical model used to describe the temperature of an asteroid, a numerical method to simulate it, a demonstration of the accuracy of the numerical model and the results we obtain.

I. Simple thermophysical model

It is useful to start presenting a physical model with a simple case. If we want to model the temperature of an asteroid in space, let us first begin with the fundamental law of thermal equilibrium:

$$Q_{in} = Q_{out} \quad (1)$$

where Q_{in} represents the solar flux heating the asteroid and Q_{out} its emission from the asteroid. The Fig. 2 describes the current situation.

The solar flux is a function depending on the distance between the asteroid to the star but also depending on the incidence angle between the direction of the sun and the normal to the surface heated:

$$Q_{in} = \frac{S_{\odot}(1 - A) \cos \varsigma}{r^2} \quad (2)$$

where S_{\odot} is the solar constant - or solar irradiance which is a flux density measuring the mean solar electromagnetic radiation per unit area, A is the albedo of the asteroid, ς is the incidence angle bounded above zero and r is the distance to the Sun in AU.



Figure 1: The binary system of asteroid Didymos viewed from the spacecraft Hera. Didymain is the biggest asteroid and Didymoon is the smallest. This image is a simulation created from Cosmographia using real data computed by NASA available with SPICE.

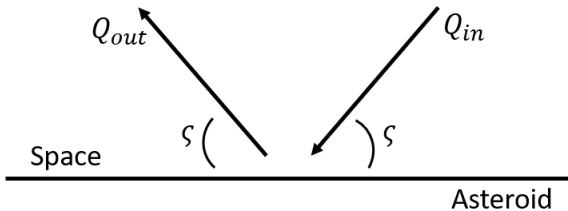


Figure 2: Asteroid thermal equilibrium model

The flux emitted from the asteroid at the thermal equilibrium is commonly written:

$$Q_{out} = \epsilon\sigma u^4 \quad (3)$$

where ϵ is the emissivity of the surface of the asteroid, σ is the Stefan-Boltzmann constant and u is the temperature of the asteroid.

Now, to find the temperature at the thermal equilibrium at one point of the surface of an asteroid, we have this formula:

$$u = \sqrt[4]{\frac{S_\odot(1-A)\cos\varsigma}{\epsilon\sigma r^2}} \quad (4)$$

It is important to insist on one point before going forward: the comparison between the local temperature at the thermal equilibrium and the global temperature at the thermal equilibrium. Firstly, the term $\frac{S_\odot}{r^2}$ in Eq. 2 and Eq. 4 with r expressed in AU is equivalent to $\frac{L_\odot}{4\pi r^2}$

with r expressed in meters. L_\odot is called the solar luminosity constant and is defined as the total power emitted from the Sun. Secondly, these equations are used to compute the local temperature at the thermal equilibrium. If ever you desire to describe the global temperature at the thermal equilibrium of the asteroid, you would rather two more infos: 1) in Eq. 2 the heated part of the asteroid is equivalent to a disk area and, 2) in Eq. 3 the area emitting is the whole spherical surface. You also want to get rid of the notion of incidence angle in Eq. 2 such as we are now talking about global temperature of a celestial body. Including these parameters would leads to equation of the global temperature at the thermal equilibrium:

$$u = \sqrt[4]{\frac{S_\odot(1-A)}{4\epsilon\sigma r^2}} \quad (5)$$

Thereby, we would use Eq. 5 to roughly approximate the whole temperature at the surface of a celestial body at the thermal equilibrium while we use Eq. 4 in this paper to describe precisely and locally the temperature at the temperature at the surface of a celestial body at the thermal equilibrium. For example, the global temperature of the Earth is around 260 K when the maximum local temperature is around 370 K , both computed at the thermal equilibrium.

We have been talking for a while about thermal equilibrium and this is what characterize the Fig. 2. But this is far from describing precisely the temperature at the surface of an asteroid. The main issue of Eq. 4 is

when the local area is not in the half side lightened of the sphere. The previous model would return a temperature of zero. What really happens is that the celestial body's dark side is cooling down while revolutioning and awaiting to get cooked again when it enters in the bright side. A better thermophysical model includes this phenomenon and mentions a ground depth which store the heat transfer. This is not an instantaneous thermal equilibrium temperature anymore but the evolution of the temperature with the notion of time, thermal inertia and thermal conduction.

II. Complete thermophysical model

The physical model that is presented in this section is a more complex model than the one seen above. It is not thermal equilibrium temperature anymore. It now includes the notion of ground depth and heat transfer. The heat flux received from the Sun on a surface area is transferred into the ground. The asteroid will keep the asteroid warmed while cooling down in the dark side. A gradient of temperatures goes from the hot to the cold. This thermophysical model is described in the equation:

$$Q_{in} = Q_{out} + Q_s \quad (6)$$

where Q_s is heat flux at the surface of the asteroid. The figure Fig. 3 represents the current situation.

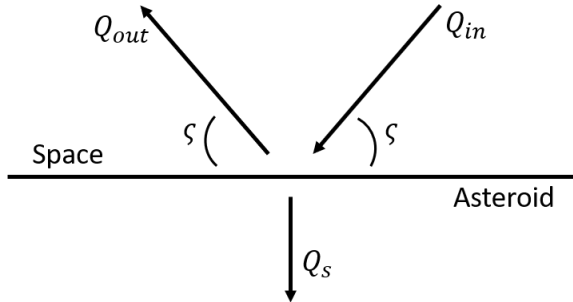


Figure 3: Asteroid thermophysical model

The heat flux at the surface of the asteroid refers to the 1D temperature gradient:

$$Q_s = -k \frac{\partial u}{\partial x} \Big|_{x=0} \quad (7)$$

where k is the conductivity of the ground of the asteroid.

We have now a heat transfer in the ground. The easiest way to model the temperature in the ground is the one-dimensional heat conduction equation:

$$u_t = \alpha u_{xx} \quad (8)$$

where u_t is the partial time derivative of the temperature, α is the diffusivity parameter and u_{xx} is the partial second space derivative of the temperature. The diffusivity defines the material property:

$$\alpha = \frac{k}{\rho c} \quad (9)$$

where ρ is the material density and c the thermal capacity of the asteroid. There are more parameters to define the properties of the ground of the asteroid and they are the thermal inertia Γ and the annual thermal skin depth l_s :

$$\Gamma = \sqrt{k\rho c} \quad (10)$$

$$l_s = \sqrt{\alpha\pi p} \quad (11)$$

where p is the orbital period of the asteroid. The thermal inertia defines the ability of the material to keep its actual temperature. The higher the thermal inertia is, the less it is impacted from temperature changes and the slowest it conducts the heat. The skin depth is considered as the depth of the ground where an adiabatic assumption can be accepted, i.e. a heat flux to zero. These material properties are generally assumed to be constants in asteroid thermophysical models but varying properties has been recently considered in some Moon, Mars, planetary satellites and asteroid models.

A numerical finite-difference technique is used to solve the 1D heat conduction equation and an iterative technique is used to solve the surface boundary condition.

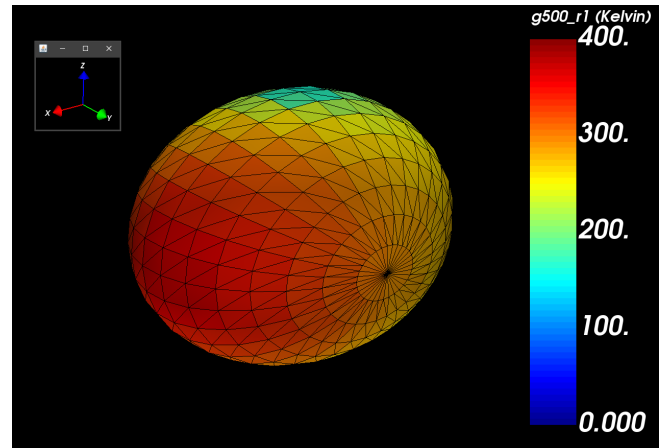


Figure 4: Example of a thermal map applied on the shape model of Didymoon.

III. Numerical method

The goal of this paper is to find a method to determine precisely the temperature at the surface of Didymoon in any situation. Since we have a realistic model from the previous section, it is now the appropriate to present a method to solve it numerically. The numerical solution uses the finite-difference technique. We call Δx and Δt the two finite-difference discretization parameters of space and time respectively. The two derivatives of

the one-dimensional heat conduction equation can be rewritten using the taylor series:

$$f(x) = \sum_{n=0}^{\infty} \frac{f^{(n)}(x_0)}{n!} (x - x_0)^n \quad (12)$$

Setting $\Delta x = x - x_0$ leads to a numerical solution of the two derivatives:

$$f''(x) \approx \frac{f(x - \Delta x) - 2f(x) + f(x + \Delta x)}{\Delta x^2} \quad (13)$$

$$f'(t) \approx \frac{f(t + \Delta t) - f(t)}{\Delta t} \quad (14)$$

Thus a numerical solution to solve the one dimensional heat conduction equation is:

$$u(x, t + \Delta t) = S(u(x - \Delta x, t) + u(x + \Delta x, t)) + (1 - 2S)u(x, t) \quad (15)$$

with,

$$S = \alpha \frac{\Delta t}{\Delta x^2} \quad (16)$$

Furthermore, the heat flux at the surface in [Eq. 6](#) and [Eq. 7](#) is solved numerically using the second order first forward derivative:

$$\left. \frac{\partial u}{\partial x} \right|_{x=0} = \frac{-u(2\Delta x, t) + 4u(\Delta x, t) - 3u(0, t)}{2\Delta x} \quad (17)$$

The equation [Eq. 6](#) can now be expressed numerically:

$$\begin{aligned} \frac{S_\odot(1 - A) \cos \varsigma}{r^2} &= \\ \epsilon \sigma u(0, t)^4 - k \frac{-u(2\Delta x, t) + 4u(\Delta x, t) - 3u(0, t)}{2\Delta x} & \end{aligned} \quad (18)$$

It is important to note that it is now impossible to isolate to one side of the equation the temperature at the surface, i.e. $u(0, t)$. A solution is to use an iterative technique to find it. We suggest the Newton's method:

$$x_{n+1} = x_n - \frac{f(x_n)}{f'(x_n)} \quad (19)$$

To get the function to implement in the Newton's method, it is necessary to move every terms of [Eq. 18](#) to one side of the equation:

$$\begin{aligned} f(x_n) &= \frac{S_\odot(1 - A) \cos \varsigma}{r^2} - \epsilon \sigma x_n^4 \\ &+ k \frac{-u(2\Delta x, t) + 4u(\Delta x, t) - 3u(0, t)}{2\Delta x} \end{aligned} \quad (20)$$

and its derivative:

$$f'(x_n) = 4\epsilon \sigma x_n^3 - \frac{3k}{2\Delta x} \quad (21)$$

The error condition in the Newton's method to find the next value of u needs to be lower than 1×10^{-5} to satisfy the stability condition of the method.

Using a finite-difference technique and iterative solution requires a suitable number of time and depth steps to fully resolve the temperature variations and to ensure the stability of the model:

$$S \leq 0.25 \quad (22)$$

Eventually, the thermophysical model can be stated:

$$\begin{cases} u(x, 0) = f(x), & \forall x \in [0, l_s] \\ u_x(0, t) = \frac{Q_{out} - Q_{in}}{k} & \forall t \geq 0 \\ u_x(l_s, t) = 0, & \forall t \geq 0 \end{cases} \quad (23)$$

where f is the intial repartition of the temperature before initiating the numerical simulation. A good choice to initialize the temperature at the beginning of a simulation is to set firstly every points to zero. The next time you run the simulation with the exact same orbital parameters and asteroid properties, you initialize every points to the values of the previous simulation, which you had cautiously saved.

This was the theory. We really have no proof whether the results of the code we can write with it will be correct or not. To prove its reliability, we need to validate some simple thermodynamical problems already solved analytically and to compare the results with our model.

IV. Validation cases

In order to trust this numerical model, it is important to prove the reliability of the method with validation cases. Please note that both methods (numerical and analytical) can only approach the reality. This part of the documents aims to study the error between existing analytical solutions and our numerical model. Let us first study the Dirichlet problem:

$$\begin{cases} u(x, 0) = f(x), & \forall x \in [0, L] \\ u(0, t) = u(L, t) = 0, & \forall t \geq 0 \end{cases} \quad (24)$$

where u is the temperature in a 1-D rod of L length and f is a function describing the intial repartition of temperature in the rod. This problem is simple because the boundary conditions are the set of temperatures. The analytical solution of this problem is based on Fourier series:

$$u(x, t) = \sum_{n=1}^{\infty} D_n \sin \left(\frac{n\pi x}{L} \right) e^{-\frac{n^2 \pi^2 \alpha t}{L^2}} \quad (25)$$

with,

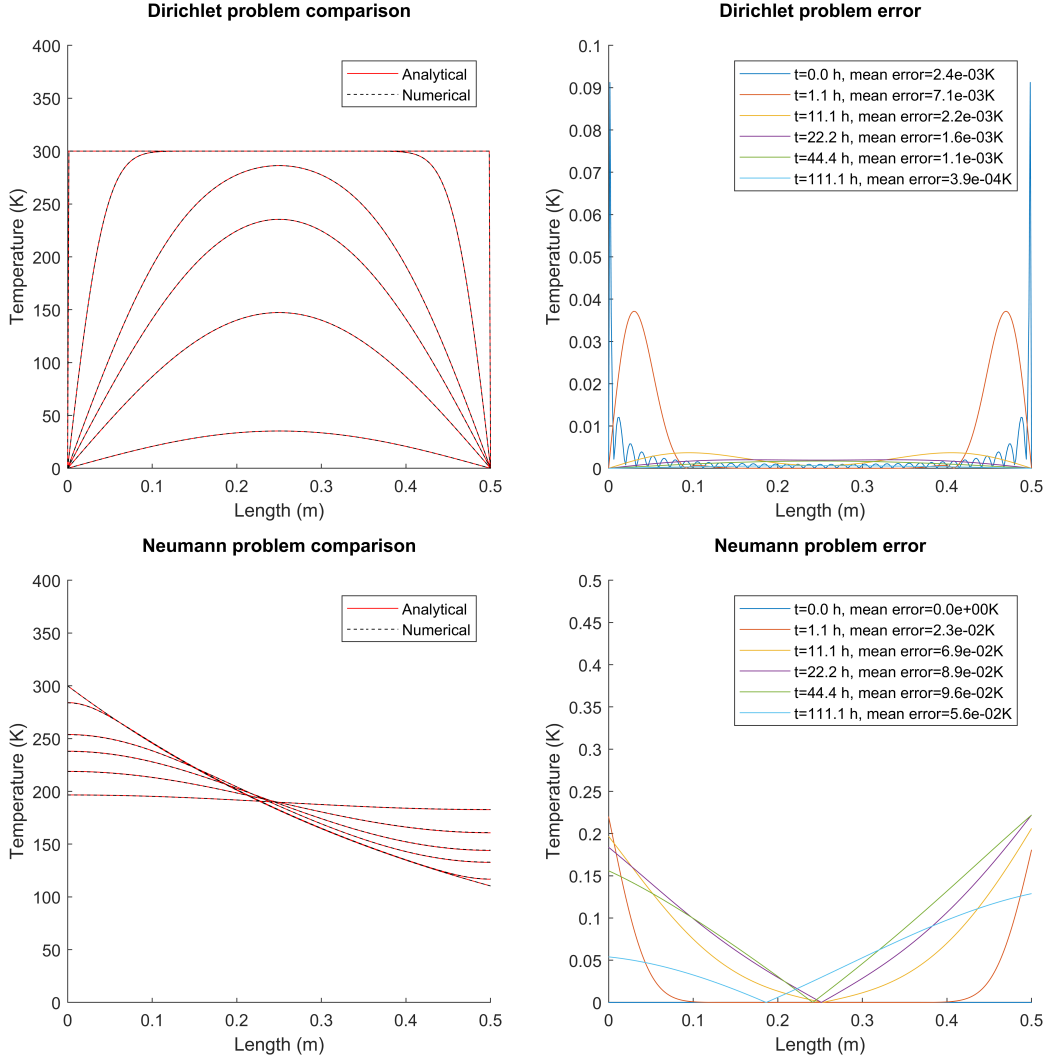


Figure 5: The two images at the top present the comparison of the results of our model with the exact solutions to the Dirichlet problem, and the two images at the bottom present those for the Neumann problem. The Dirichlet problem was initialized with a constant 300 K in the rod and with both side at 0 K. We can observe the boundary conditions of temperatures of the Dirichlet problem as both side stay at 0 K. Fixing both sides temperatures leads the heat flux to get temperatures leaving the rod. We can indeed observe temperatures in the rod descreasing everywhere. The Neumann problem was initialized in Eq. 32. We observe the boundary conditions of flux for the Neumann problem with leads the temperature to reach the mean value. The two graphs at the left for both problem show the accuracy of the numerical model because both curves are superimposed. The two graphs at the right describe how precise the model really is. The value of N to define the analytical method as been set to 1×10^5 and increasing the value does not change the results. The time step is 4 s and the depth step is 1.6 mm. Asteroid thermal properties are listed in Tab. 1 with respect of the stability condition.

$$D_n = \frac{2}{L} \int_0^L f(x) \sin\left(\frac{n\pi x}{L}\right) dx \quad (26)$$

We compute the error between the numerical model and the analytical solution:

$$E = \frac{1}{N_x} \sum_{x=0}^L |u(x, t) - u_{exact}(x, t)| \quad (27)$$

with N_x the number of x subdivisions.

The figure Fig. 5 shows the application of both the numerical method and the analytical solution to the Dirichlet problem, and the difference between the two of them. The results are described under the figure. From these results, it can be concluded that the numerical method can be fully trusted to solve this kind of problem. The Dirichlet problem was a simple case but not the exact one studied in this document in the case of the asteroid. The exact problem is about setting a condition on the heat flux of both side and not about setting the temperature. There exists a study case with an existing solution to our problem, it is called: the Neumann problem. By setting the flux to zero, it models a concrete temperature equilibrium phenomenon in a surface. Thus, the final temperature in the rod after the simulation will be approximately a mean temperature of the initial condition at time zero. The Neumann problem is written:

$$\begin{cases} u(x, 0) = f(x), & \forall x \in [0, L] \\ u_x(0, t) = u_x(L, t) = 0, & \forall t \geq 0 \end{cases} \quad (28)$$

The solution of the Neumann problem is slightly different to the Dirichlet problem to satisfy the conditions of the problem,

$$u(x, t) = \sum_{n=0}^{\infty} B_n e^{-k\left(\frac{n\pi}{L}\right)^2 t} \cos\left(\frac{n\pi}{L}x\right) \quad (29)$$

where,

$$B_n = \frac{2}{L} \int_0^L f(x) \cos\left(\frac{n\pi}{L}x\right) dx \quad (30)$$

$\forall n \geq 1$

and,

$$B_0 = \frac{1}{L} \int_0^L f(x) dx \quad (31)$$

Lets us take an initial temperature in the rod different a bit more complex than a single constant line, for instance,

$$f(x) = T_0 e^{-xb} \quad (32)$$

The Fig. 5 also shows the application of both the numerical method and the analytical solution to the Neumann problem, and the difference between the two of them. The results are described under the figure. From

these results, it can be concluded that the numerical method can be fully trusted to solve this kind of problem too, which is the exact same problem as the one studied in this document.

From those two study cases, it makes sense to conclude that our numerical model can be trusted. It is now possible to apply the model to the purpose of this paper, i.e. modeling the temperature at the surface of Didymoon.

V. Application and results

The physics to model the temperature at the surface of an asteroid has been presented earlier in this document. We then introduced a numerical method to model it. We also proved the reliability of the numerical model by comparing it with exact solutions of several known problems. We now aim in this section to gather all the tools we have developed in previous sections to achieve the purpose of this paper which is modeling the temperature at the surface of Didymoon. To start we want simple cases to observe coherent results and we will compare them with results of existing papers. We begin with the assumption of a spherical asteroid located at fixed distance to the Sun on the ecliptic plane without obliquity. We already take into account asteroid revolution because it has an immediate impact on the evolution of the asteroid temperature, but Didymoon's obliquity will not be introduced before Fig. 9. Thus, the temperature of a single point at the equator on the surface at the thermal equilibrium is shown in Fig. 6. The convergence of the model is studied in Fig. 7. The model of the heat conduction within the ground is presented in Fig. 8. The Fig. 9 points out the influence of distance to the Sun on the asteroid temperature and compares our results with Ref. 1. The Fig. 10 shows the influence of the asteroid thermal inertia on its temperature and compares our results with Ref. 2. The temperature of the whole asteroid is modelled with contour maps in Fig. 11.

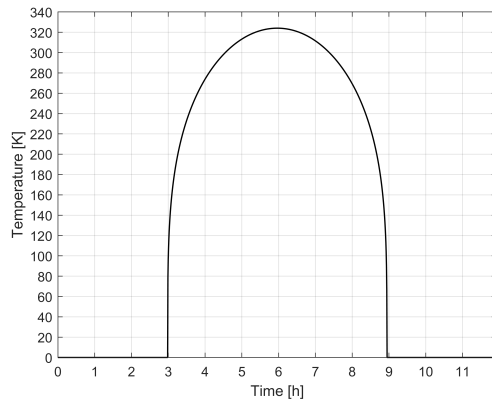


Figure 6: Thermal equilibrium temperatures on the equator of spherical asteroid located on the ecliptic plane at 1.5 AU to the Sun. Other asteroid properties are listed in Tab. 1.

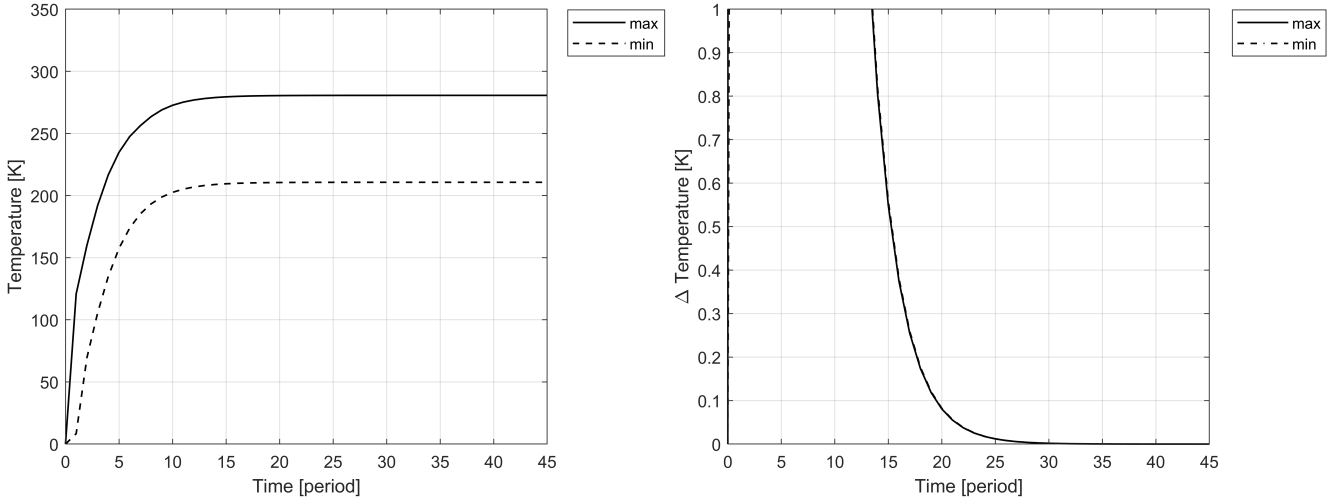


Figure 7: Temperatures convergence evolution after several periods for a ground depth of one annual thermal skin depth (see Eq. 11). The right plot shows the evolution of the difference of temperature. The numerical method needs 20 revolutions to get less than 0.1 kelvins of error with the exact value. The asteroid was a sphere located at 1.5 AU to the Sun. Other asteroid properties are listed in Tab. 1.

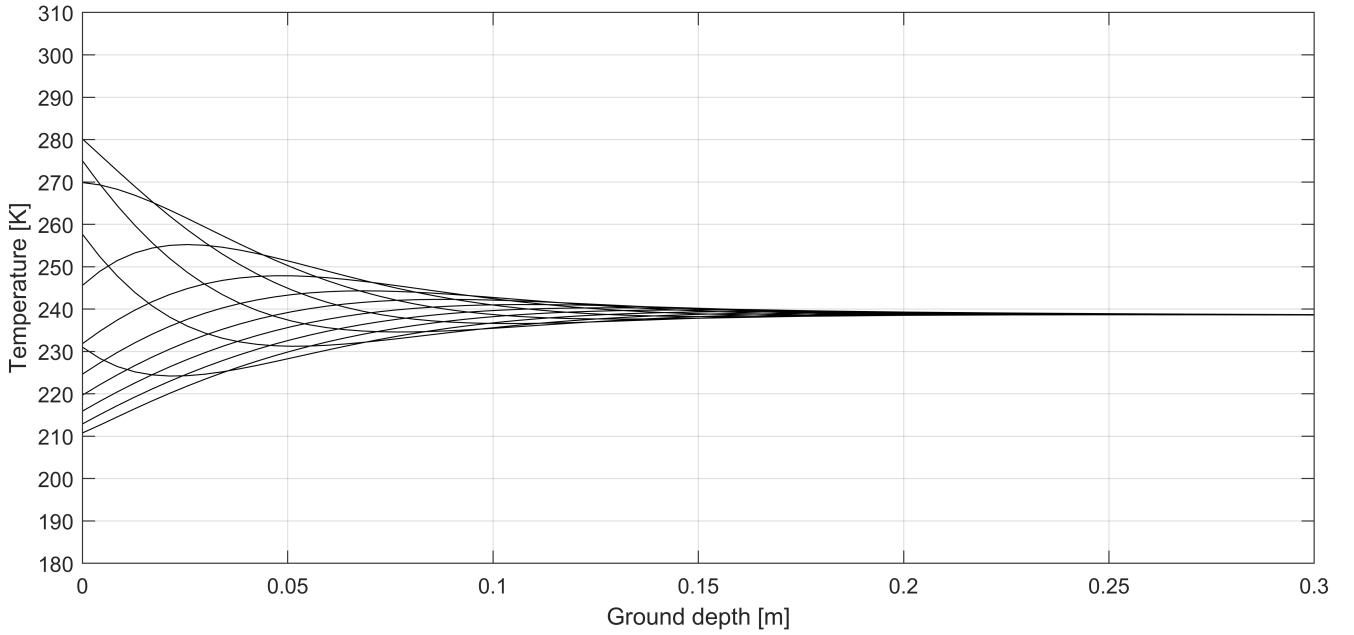


Figure 8: Equator ground temperatures of spherical asteroid at 1.5 AU to the Sun. Other asteroid properties are listed in Tab. 1. Each line is separated from one hour and the whole covers a full revolution period. Exact ground temperature requires several annual thermal skin depth and after 0.3 meters the temperature is stable enough.

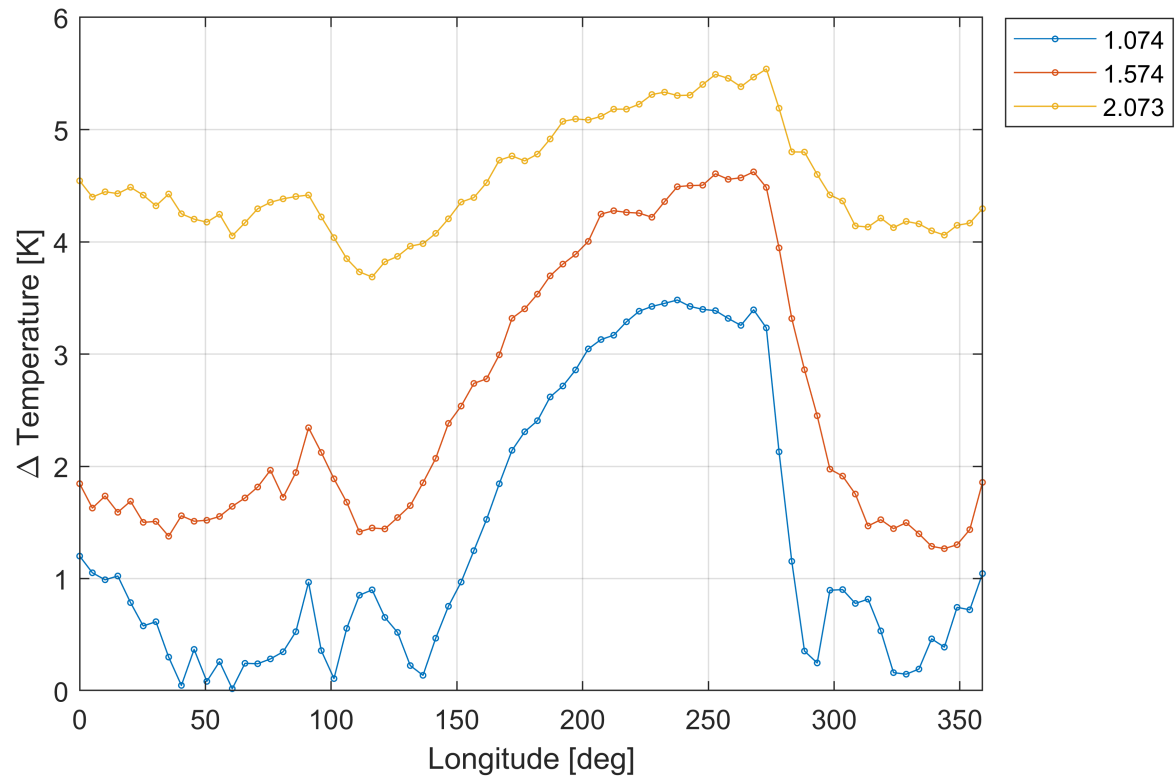
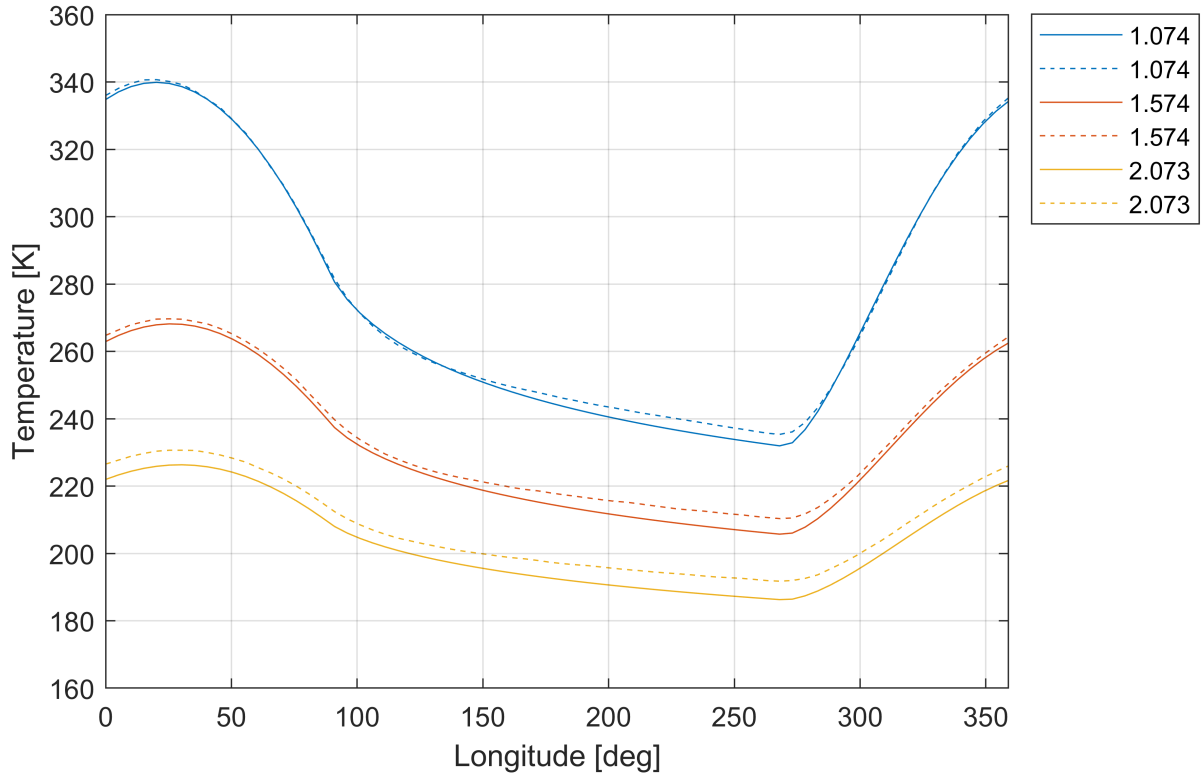


Figure 9: Heliocentric distance influence on equator surface temperatures around spherical asteroid. Legend contains different distances to the Sun in AU and dashed lines are the results of Ref. 1. Asteroid properties are listed in Tab. 1. Didymoon obliquity is included in this simulation.

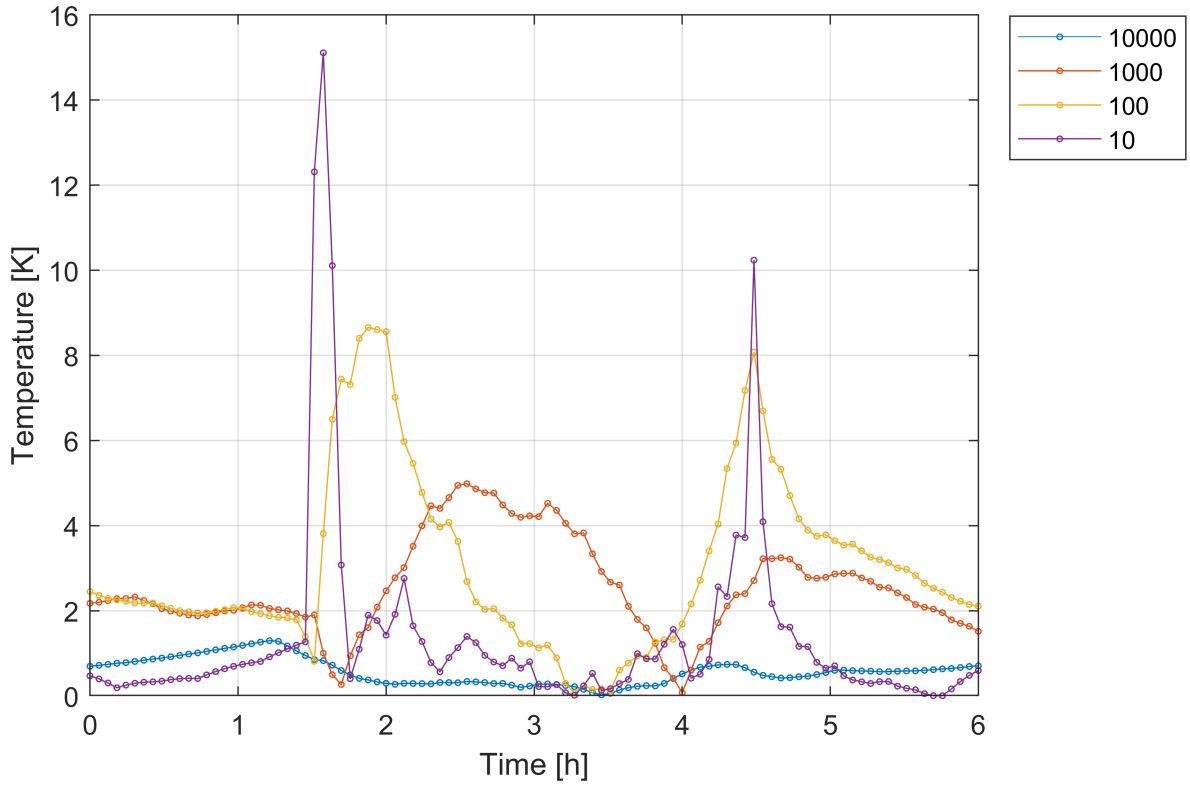
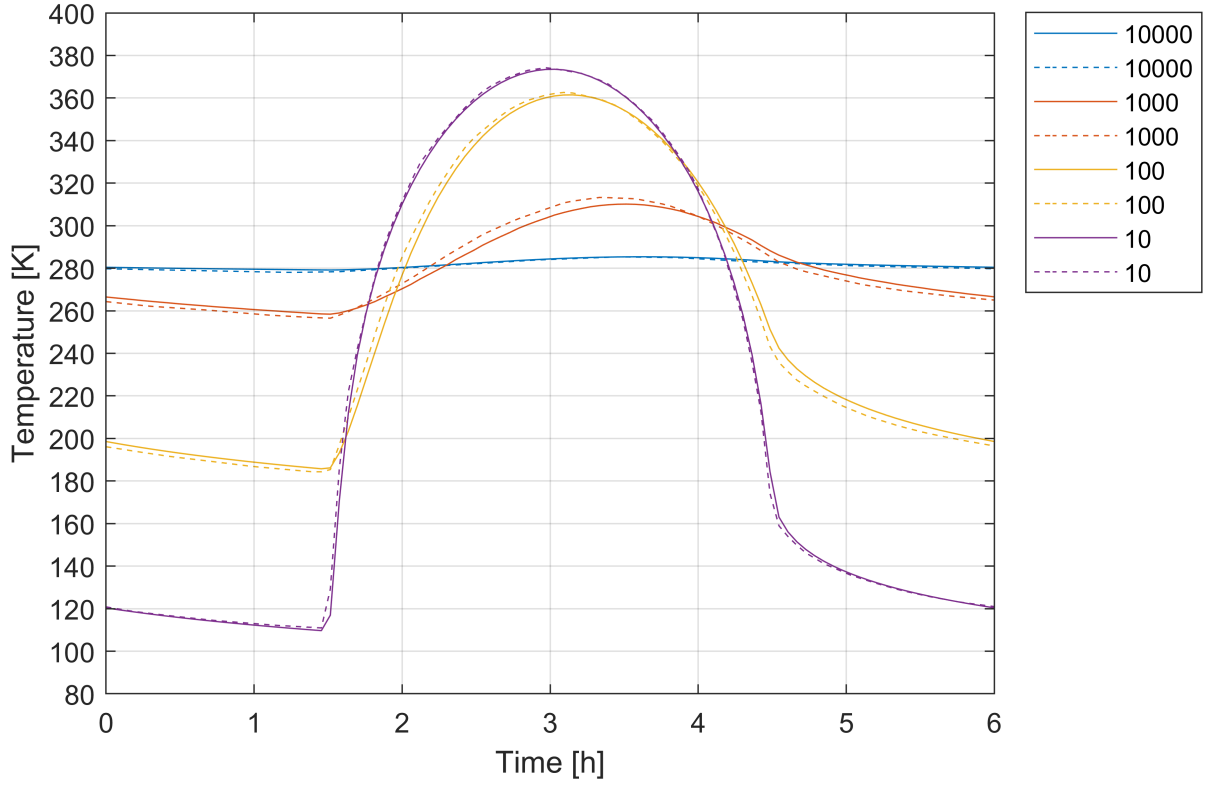


Figure 10: Thermal inertia influence on equator surface temperatures around spherical asteroid. Legend contains different thermal inertias and dashed lines are the results of Ref. 2. Asteroid is at 1.1 AU to the Sun with albedo of 0.1 and without obliquity. Other asteroid properties are listed in Tab. 1.

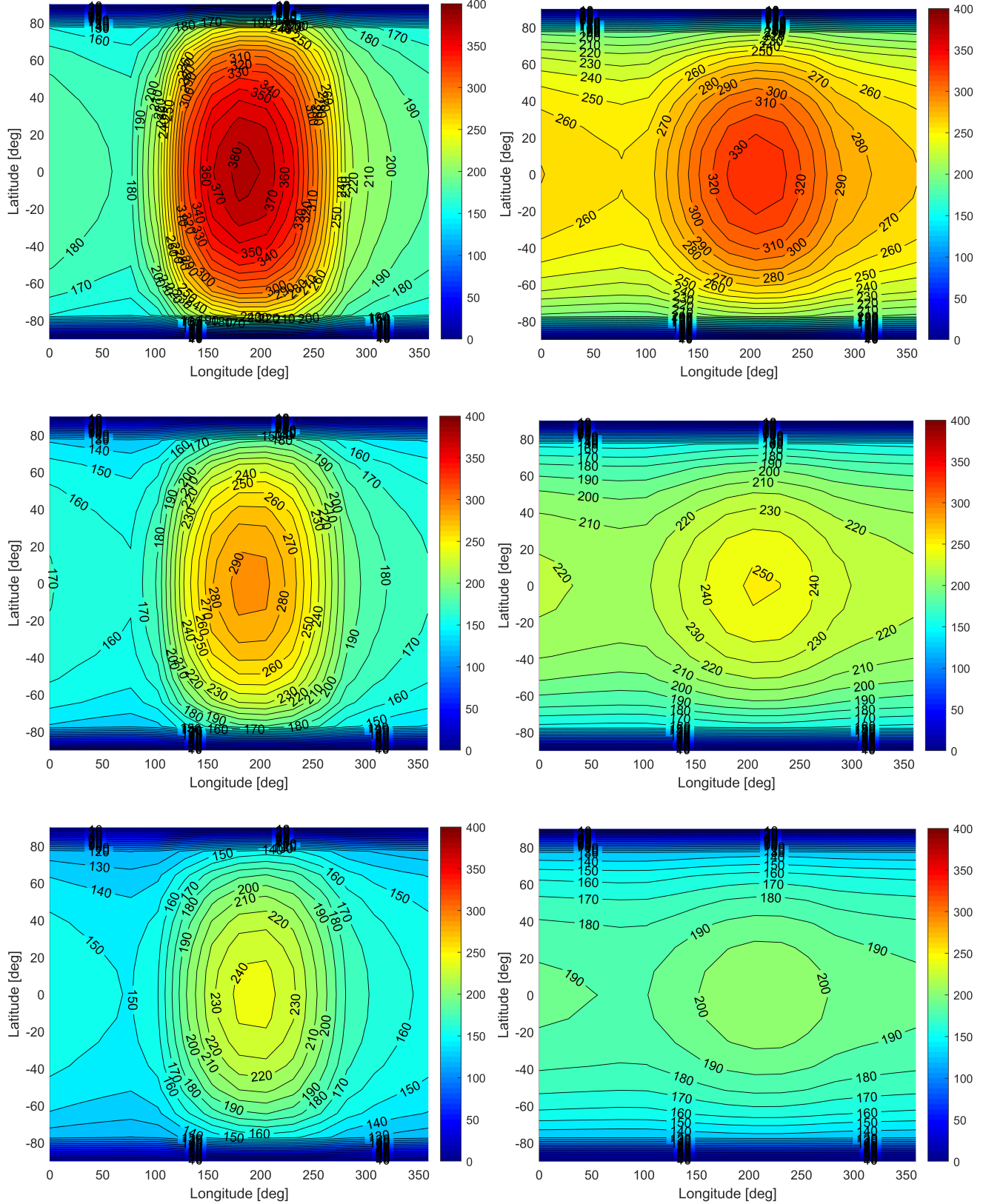


Figure 11: Contour map of the temperature of a spherical asteroid for extreme thermal inertia (from the left to the right: 100, 1000) and for closer and larger distance to the Sun (from the top to the bottom: 1.0131 AU, 1.6643 AU, 2.2754 AU), without obliquity. Other asteroid properties are listed in [Tab. 1](#).

VI. Hera observation data with SPICE

To go further in this document, we propose to study the future observations of the Hera spacecraft instruments with the objective to prepare as well as possible the mission. Data are computed by the ESA the NASA and gathered on SPICE. We will firstly study important parameters in the [Fig. 12](#) such as the distance from Hera to Didymoon throughout the time, the phase angle between the observation vector of the Hera camera pointing to Didymos and the solar angle on Didymoon, and see when Didymoon is in the field of view (FOV) of the Hera camera. Data available were computed for a short period in 2027 from January to June. During this period, we identify 4 important different phases, the ECP phase from January 28th to February 25th, the DCP1 phase from February 25th to March 28th, the DCP3 phase from April 25th to June 24th, and eventually the DCP3VCF phase from June 3rd to June 6th.

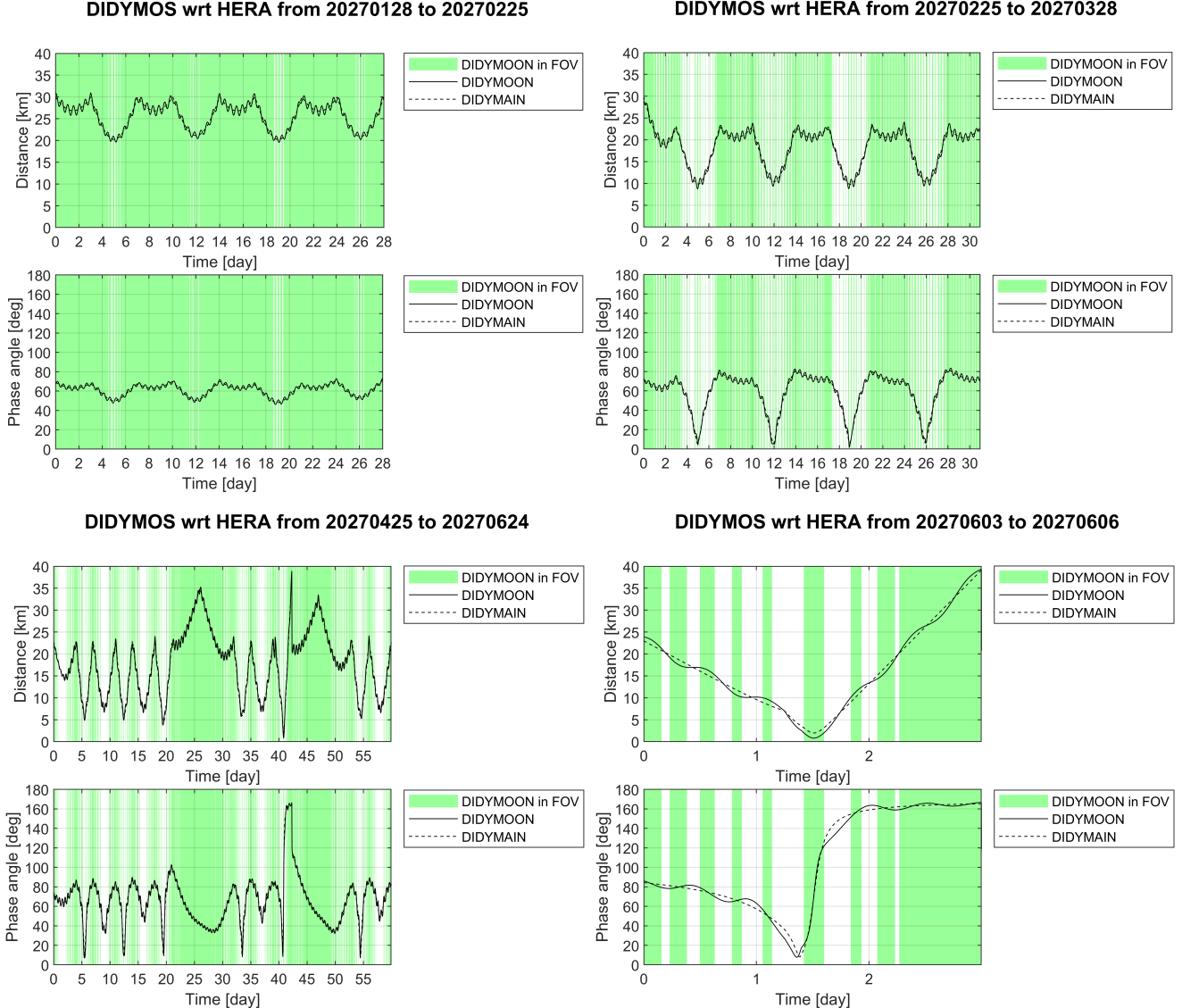
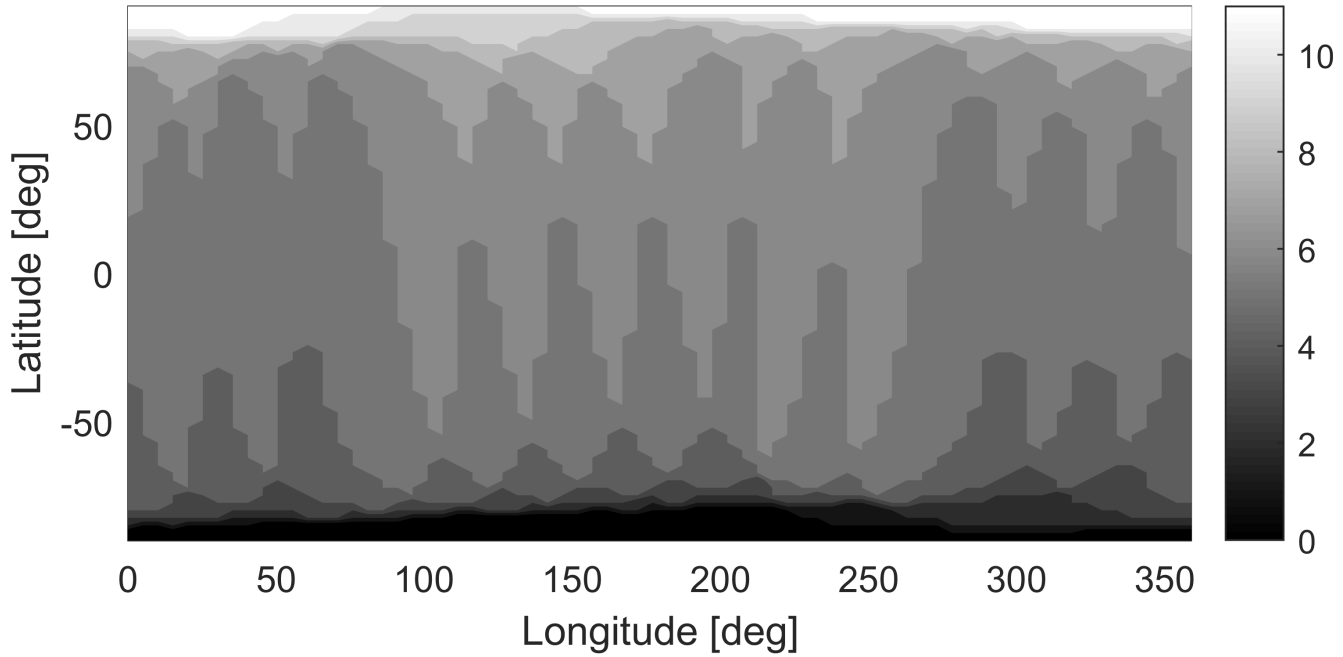


Figure 12: *Didymos asteroids binary system distance, phase angle and FOV with respect to Hera spacecraft for the 4 different phase periods. Didymain is always in Hera camera field of view because the spacecraft sensor points toward it. Thus, depending on the distance and because Didymoon orbits around Didymain, Didymoon is not always in the field of view of the Hera camera.*

DIDYMOON visible area wrt HERA on 2027-FEB-05 06:50:00



DIDYMOON visible area wrt HERA on 2027-JUN-05 02:35:00

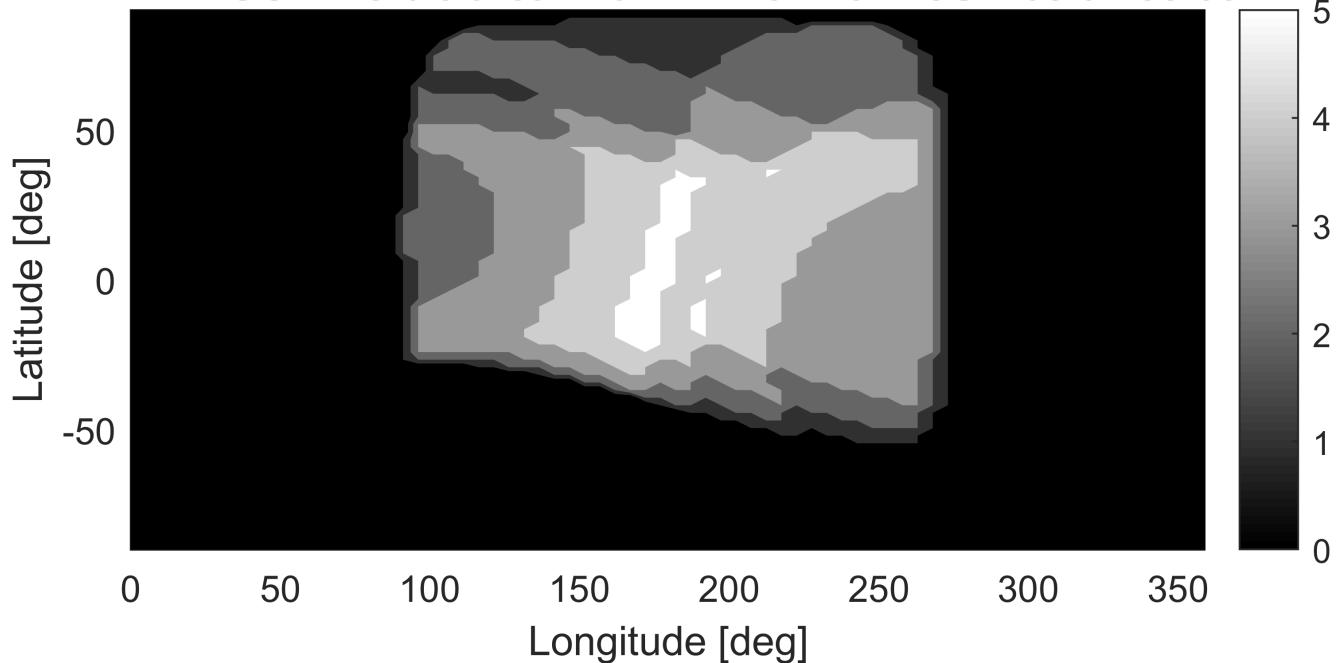


Figure 13: Didymosurface visible area view from the Hera camera. The first graph is 12 images taken during a full orbital period of Didymosurface, and the second graph is 6 images taken during a passage of 1 hour of Didymosurface in the Hera camera FOV. Eclipses included.

Tables

Name	Symbol	Value	Units
Stefan-Boltzman constant	σ	$5.670\,374\,419 \times 10^{-8}$	kg s^{-1}
Solar constant	S_{\odot}	1361.5	W m^{-2}
Solar luminosity constant	L_{\odot}	3.846×10^{26}	W
Bond albedo	A	0.07	
Emissivity	ϵ	0.9	
Thermal inertia	Γ	500	$\text{J K}^{-1} \text{m}^{-2} \text{s}^{-\frac{1}{2}}$
Density	ρ	2146	kg m^{-3}
Heat capacity	c	600	J K^{-1}
Orbital period	p_o	11.92	hour
Revolution period	p_r	11.92	hour
Obliquity	δ	162	degree

Table 1: Table of the constants used in this document.

References

- [1] Ivanka Pelivan, Line Drube, Ekkehard Kührt, Jörn Helbert, Jens Biele, Michael Maibaum, Barbara Cozzoni, Valentina Lommatsch, *Thermophysical modeling of Didymos' moon for the Asteroid Impact Mission*, 2017.
- [2] Marco Delbo, Michael Mueller, Joshua P. Emery, Ben Rozitis, Maria Teresa Capria, *Asteroid Thermophysical modeling*, 2016.
- [3] European Space Agency, *Asteroid Impact Mission: Didymos Reference Model*, 2015.
- [4] Elodie Glosesener, *Methane clathrate hydrate stability in the martian subsurface and outgassing scenarios*, 2019.